Polish Journal of Radiology
w w w . P o l R a d i o l . c o m

ORIGINAL ARTICLE

Diagnostic Accuracy of Gd-EOB-DTPA for Detection Hepatocellular Carcinoma (HCC): A Comparative Study with Dynamic Contrast Enhanced Magnetic Resonance Imaging (MRI) and Dynamic Contrast Enhanced Computed Tomography (CT)

Authors' Contribution:
A Study Design
B Data Collection
C Statistical Analysis
D Data Interpretation
E Manuscript Preparation
F Literature Search
G Funds Collection

Massimo Imbriaco[1A], Serena De Luca[1E], Milena Coppola[1C], Mario Fusari[1E], Michele Klain[1A], Marta Puglia[1D], Pierpaolo Mainenti[2E], Raffaele Liuzzi[2G], Simone Maurea[1A]

[1] Department of Advanced Biomedical Sciences, University "Federico II", Napoli, Italy
[2] Institute of Biostructure and Bioimaging, National Research Council (CNR), Napoli, Italy

Author's address: Massimo Imbriaco, Department of Advanced Biomedical Sciences, University "Federico II", Via Pansini, 5, 80123, Napoli, Italy, e-mail: mimbriaco@hotmail.com

Summary

Background: To compare the diagnostic accuracy of hepato-biliary (HB) phase with gadolinium-ethoxybenzyl-diethylenetriamine-pentaacetic acid (Gd-EOB-DTPA) with dynamic contrast-enhanced MR imaging (DCEMRI) and contrast-enhanced CT (DCECT) for hepatocellular carcinoma (HCC) detection.

Material/Methods: 73 patients underwent DCECT and Gd-EOB-DTPA-3T-MR. Lesions were classified using a five-point confidence scale. Reference standard was a combination of pathological evidence and tumor growth at follow-up CT/MR at 12 months. Receiver Operating Characteristic (ROC) curves were obtained.

Results: A total of 125 lesions were confirmed in 73 patients. As many as 74 were HCCs and 51 were benign. Area under the curve (AUC) was 0.984 for DCEMRI+HB phase *vs.* 0.934 for DCEMRI ($p<0.68$) and 0.852 for DCECT ($p<0.001$). For lesions >20 mm (n.40), AUC was 0.984 for DCEMRI+HB phase, 0.999 for DCEMRI, and 0.913 for DCECT, (p=n.s.). For lesions <20 mm (n.85) AUC was 0.982 for DCEMRI+HB phase *vs.* 0.910 for DCEMRI ($p<0.01$) and 0.828 for DCECT ($p<0.001$).

Conclusions: The addition of HB phase to DCEMRI provides an incremental accuracy of 4.5% compared to DCEMRI and DCECT for HCC detection. The accuracy of Gd-EOB-DTPA-3T-MR significantly improves for lesions <20 mm. No significant improvement is observed for lesions >20 mm and patients with Child-Pugh class B or C.

MeSH Keywords: Contrast Media • Liver Neoplasms • Magnetic Resonance Imaging • Tomography Scanners, X-Ray Computed

PDF file: http://www.polradiol.com/abstract/index/idArt/899239

Background

Hepatocellular carcinoma (HCC) is the fifth most common tumor worldwide and the third most common cause of cancer-related death, after lung and stomach cancer [1]. HCC is the main cause of death among cirrhotic patients and the incidence is predicted to increase in the next two decades [2]. According to the American Association for the Study of Liver Diseases (AASLD), dynamic computed tomography (CT) and magnetic resonance imaging (MRI) are the best imaging modalities currently available in the diagnostics and staging of HCC [3,4]. Although CT scan is

the most widely used imaging technique for HCC detection and staging, in the last years the MRI "liver-specific" contrast agents such as gadolinium-ethoxybenzyl-diethylenetriamine-pentaacetic acid (Gd-EOB-DTPA), also known as gadoxetate disodium/gadoxetic acid (Primovist, Eovist, Bayer Schering Pharma, Germany) are playing a crucial role in detection and characterization of hepatic lesions.

Considering its more favorable pharmacokinetic and pharmacodynamic properties [5] and the reported higher sensitivity in identifying hepatocellular carcinoma [6], Gd-EOB-DTPA seems to be the most helpful diagnostic tool in predicting carcinogenesis in cirrhotic liver and particularly in identifying a significant proportion of HCCs that are non-hypervascular, and that may be misclassified using standard criteria [7].

The added value of Gd-EOB-DTPA is a combination of the properties of a conventional extracellular contrast agent with those of a liver-specific contrast agent. After a dynamic phase, Gd-EOB-DTPA accumulates in functioning hepatocytes in the delayed phase which begins 10 minutes after injection, earlier than with Gd-BOPTA [8,9].

In the hepatocyte phase, typical HCCs are well described as areas of low signal intensity relative to the surrounding liver parenchyma because they do not have the ability to take up Gd-EOB-DTPA [10–13]. Otherwise, it has also been shown that some HCCs exhibit iso/hyperintensity on hepatobiliary phase imaging compared to the normal parenchyma.

The aim of the present study was to evaluate the diagnostic accuracy of hepato-biliary (HB) phase MRI with Gd-EOB-DTPA, compared with that of dynamic contrast-enhanced magnetic resonance imaging (DCEMRI) and dynamic contrast-enhanced CT (DCECT), for detection of HCC in patients with liver cirrhosis.

Material and Methods

Informed consent, a requirement of the protocol approved by the Institutional Clinical Research Subpanel on Human Studies at our Institute, was obtained from all patients. Between June 2012 and January 2014, seventy-three cirrhotic patients (50 men, 23 women; mean age, 60 years; age range, 41–81 years) underwent multiphasic 64-section multi-detector CT and gadoxetate disodium–enhanced MR imaging, in a prospective fashion. The sample size was calculated in order to obtain a statistical power of 80%. Clinical characteristics of patients enrolled in the study are shown in Table 1. Inclusion criteria were suspicious findings on US and increased laboratory parameters (e.g., alpha-fetoprotein). Exclusion criteria were renal failure, allergy to contrast agents, hyperthyroidism, pregnancy and for the MRI examination, pacemaker or other non-compatible implants and claustrophobia.

The imaging examinations were performed within one month of each other due to experimental setting. Two radiologists, blinded to pathology results, independently evaluated unenhanced and dynamic phases for CT, and unenhanced, dynamic, and HB phases for MRI obtaining three

Table 1. Demographic and clinical characteristics of patients.

Number of patients	73	
Age (years)		
Mean ±SD	60±8.2	
Range	41–81	
Gender		
Men	50	(68%)
Women	23	(32%)
Cause of cirrhosis		
HCV	56	(78%)
HBV	9	(12%)
HBV/HDV	4	(5%)
Alcohol abuse	3	(4%)
Other	1	(1%)
Child-Pugh Class		
A	38	(52%)
B	20	(27%)
C	15	(21%)

sets of images. Readers classified all detected lesions on CT and MRI with the use of a five-point confidence scale, assuming lesions scored 1 and 2 as benign and lesions scored from 3 to 5 as malignant. The final diagnosis was obtained by a combination of pathological proof confirmed by percutaneous needle biopsy, combined imaging findings, and substantial tumor growth at follow-up CT or MR imaging (range of follow-up, 12 months).

Computed Tomography Imaging

CT examinations were performed using a 64-detector row CT scanner (Aquilion 64, Toshiba Medical Systems). Unenhanced baseline scan of the liver was obtained using the following parameters: collimation=1×32 mm; table feed=36 mm/s; rotation time=0.75 seconds; thickness reconstruction=5 mm; 120 kVp; hepatic arterial phase (HAP) started 30–35 seconds after the administration of contrast material. A portal venous phase (PVP) of the abdomen and pelvis started 40 seconds after the end of the HAP acquisition and equilibrium phase of the upper abdomen, at 180 seconds. Nonionic iodinated contrast agent (Iopromide, Ultravist 370 mgI/mL Schering AG, Berlin, Germany) was injected at a rate of 3 mL/sec.

Magnetic Resonance Imaging

MR studies were performed with a 3-Tesla scanner (Magnetom Trio, Siemens Medical System, Germany). All patients were studied with dedicated T1- and T2-weighted sequences using a phased-array synergy body coil. Routine liver MRIs were acquired using the following sequences: pre-contrast triggered HASTE (Half-Fourier Acquired

Table 2. Diagnostic performance for characterization of HCC between DCECT and DCEMRI.

Parameter	DCECT	DCEMRI	p value
Sensitivity	76%	93%	0.006
Specificity	86%	94%	0.029
Diagnostic accuracy	81%	94%	0.037
Positive predictive value	87%	95%	0.141*
Negative predictive value	76%	92%	0.03

DCECT – dynamic contrast-enhanced CT; DCEMRI – dynamic contrast-enhanced MRI; confidence intervals 95%; * not significant.

Table 3. Diagnostic performance for characterization of HCC between DCEMRI and DCEMRI+HB phase.

Parameter	DCEMRI	DCEMRI+HB phase	p value
Sensitivity	93%	95%	0.688*
Specificity	94%	100%	0.25*
Diagnostic accuracy	94%	98%	0.52*
Positive predictive value	95%	100%	0.08*
Negative predictive value	92%	96%	0.513*

DCEMRI – dynamic contrast-enhanced MRI; DCEMRI+HB phase – dynamic contrast-enhanced MRI + hepato-biliary phase; confidence intervals 95%; * not significant.

Single-Shot turbo Spin-Echo) T2-weighted in coronal and axial planes, TE 2000 ms, TR 90 ms, slice thickness 5 mm; axial T2 HASTE in coronal plane Fat Saturated. HASTE T1-weighted in axial planes, TE 2 ms, TR 1500 ms, slice thickness 5 mm; two breath-hold T1-weighted spoiled gradient recalled echo (GRE) in-phase sequences (TR 140 ms, TE 1.22 ms) and out-of-phase (TR 150 ms, TE 2.5 ms), slice thickness 5 mm. Contrast-enhanced sequences were performed using a three-dimensional (3D) VIBE (Volumetric Interpolated Breath Hold Examination) dynamic technique with fat saturation and antecubital intravenous administration of 0.025 mmol/kg body weight of Gd-EOB-DTPA (Primovist, Bayer Shering Pharma A, Berlin, Germany) with an injection rate of 2 mL/sec followed by a 30-mL saline flush. The multiphase dynamic technique included an arterial (25–35 s), portal (70–80 s) and delayed (180 s) phase. The MRI parameters were: TR 3.3 ms, TE 17 ms, slice thickness 2 mm. Finally, the HB phase was obtained 15 min after the beginning of contrast medium administration with the same parameters of dynamic imaging.

Image analysis

Images were reviewed separately by two radiologists (M.I, S.M) with more than 15 years of experience in liver imaging. The two readers evaluated the images independently and were blinded to patients' clinical and ultrasonographic findings. In case of discordant interpretation of the CT and/or MR images, a third reader was invited to provide an additional evaluation. A further evaluation of dynamic MRI was assessed including also the images of HB phase using a different score system based on a positive/uncertain/negative score in relation to the ipo/iso/iper-intensity of the lesion in this specific phase. For each imaging

modality, the diagnostic accuracy was assessed by measuring the area under the curve (AUC) of the free-response Receiver Operating Characteristic analysis (ROC) on a lesion-per-patient-basis. Diagnostic accuracy, sensitivity, specificity, PPV, and NPV, with corresponding 95% confidence intervals, were determined for characterization of HCCs and compared among the three sets of images. The differences in the ROC-curve, were statistically analyzed using Mc Nemar test and Z test. In particular, we tested whether there was a statistically significant difference between results provided by the three imaging modalities, as confirmed by the reference standards. P values <0.05 were considered significantly different. Furthermore, we evaluated inter-reader agreement by Kappa values with 95% confidence intervals.

Results

A total of 73 patients with clinical diagnosis of liver cirrhosis (Child-Pugh A–C) were included in this study (52% Child-Pugh class A, 27% Child-Pugh class B and 21% Child-Pugh class C). As many as 125 hepatic lesions were confirmed in 73 patients. Of the 125 hepatic lesions, 74 HCCs (mean size 22 mm, range 6–42 mm) were pathologically confirmed by percutaneous needle biopsy in 38 patients; conversely, 51 benign lesions (mean size 14 mm, range 5–31 mm) in 35 patients, were confirmed by either pathological diagnosis (12 regenerative nodules; 9 dysplastic nodules, 3 siderotic nodules, 1 focal nodular hyperplasia) or by combined imaging criteria with more than 12 months' follow-up (9 cysts, 7 hemangiomas, 6 arterial-venous shunts, 4 areas of necrosis following tumor ablation). Using the combined imaging criteria, a lesion was diagnosed as hemangioma (n=7) if it showed: (a) peripheral contrast

enhancement on the HAP of CT images and residual contrast enhancement on the equilibrium phase CT images; (b) peripheral contrast enhancement on the HAP and marked hyperintensity on T2-weighted MR imaging; and c) findings of (b) remained unchanged for more than 12 months. The lesion was diagnosed as an arterial-venous shunt (n=6) if it: (a) showed a wedge shape, early enhancement on HAP of CT or MR imaging, and isodensity/isointensity on PVP and equilibrium phase images and (b) disappeared on follow-up studies or remained unchanged for more than 12 months. A diagnosis of other benign lesion was made if neither the criteria for hemangioma nor arterial-venous shunts were fulfilled and no changes were observed at follow-up CT or MR imaging, for more than 12 months.

Table 2 summarizes the overall results of comparison between DCECT and DCEMRI. Sensitivity, specificity, diagnostic accuracy, PPV and NPV were significantly higher ($p<0.05$) for DCEMRI compared to DCECT: 93–76%, 94–86%, 94–80%, 95–86%, 92–76% (CI: 95%). The addition of HB to DCEMRI provided an incremental value of 2% for sensitivity ($p=0.68$), 6% for specificity ($p=0.25$), 4.5% for diagnostic accuracy ($p=0.52$), 5% for PPV ($p=0.08$) and 4% for NPV ($p=0.5$), as shown in Table 3. The combined reading of both sets increased the diagnostic accuracy of the readers, particularly because of the highest reliability in excluding false-positive results. Inter-reader agreement was good (Kappa=0.80). Examples of comparison among DCECT, DCEMRI and HB phase-enhanced MRI are shown in Figures 1 and 2. ROC curves for DCECT, DCEMRI and HB phase-enhanced MRI are illustrated in Figure 3A–3C. Overall, the highest absolute AUC value was 0.984 for DCEMRI+HB phase *vs.* 0.934 for DCEMRI ($p<0.68$) and 0.852 for DCECT ($p<0.001$) (Figure 3A). In a sub-group analysis of lesions >20 mm (n. 40), no significant differences were observed among the three imaging modalities with AUC values respectively of 0.984 for DCEMRI+HB phase, 0.999 for DCEMRI, and 0.913 for DCECT (Figure 3B). Conversely, for lesions <20 mm (n. 85) AUC values were respectively of 0.982 for DCEMRI+HB phase *vs.* 0.910 for DCEMRI ($p<0.01$) and 0.828 for DCECT ($p<0.001$) (Figure 3C).

Discussion

The results of this study demonstrate an incremental diagnostic accuracy of Gd-EOB-DTPA-enhanced MRI compared to DCEMRI and DCECT for HCC detection. The accuracy of Gd-EOB-DTPA-3T-MR significantly improves for lesions <20 mm. No significant improvement is observed for lesions >20 mm and patients with Child-Pugh class B or C.

Contrast-enhanced MRI plays a major role in the characterization of focal liver lesions [4]. Due to its greater contrast resolution MRI allows an easier identification and characterization of liver lesions, compared to CT imaging [14]. In patients with a high degree of cirrhosis, the enhancement of the liver parenchyma during HB phase is reduced compared to the healthy liver due to the fact that hepatocyte damage, associated with vascular abnormalities and the presence of nodules of fibrosis cause an alteration of the normal capacity of hepatocytes to capture the GD-EOB-DTPA from their sinusoidal side and secrete it through the biliary pole [15–17].

These findings have been demonstrated especially for lesions 2 cm in diameter or smaller [18]. In our series the addition of HB phase to DCEMRI provided an overall incremental diagnostic accuracy of 4.5%, confirming the trend of a superior lesion conspicuity compared to DCEMRI alone. Our results are in agreement with previous data by Cha et al. [19], showing the higher diagnostic accuracy of high field MRI combining thinner section acquisitions, with improved background suppression and greater sensitivity to gadolinium chelates using high magnetic field strength as 3T. This better image quality has important clinical implications, the detection of small HCCs can lead to potentially curative treatments, such as radical approaches including resection and transplantation for early BCLC stage or radiofrequency ablation [3]. The diagnostic contribute in characterization of HCC of the HB phase imaging with GD-EOB-DTPA is another matter of big concern.

For our DCEMRI we chose to administer GD-EOB-DTPA with the aim to assess the added value of the hepato-biliary phase in characterizing and identifying focal liver lesions in our high-risk population. We found an improved diagnostic accuracy of DCEMRI plus HB phase imaging at 20 minutes compared to the DCEMRI alone. In particular, in our series in a sub-group analysis of lesions <20 mm (n. 85), we observed a significantly improved diagnostic accuracy of HB enhanced DCEMRI compared to DCEMRI alone. Conversely, in 40 lesions with a maximum diameter >20 mm, no significant differences were observed among the three imaging modalities. Absence of statistically significant contribution of HB phase in characterizing focal liver lesions for lesions >20 mm, can be explained by the characteristics of our study population, with a high percentage of patients belonging to Child-Pugh class B (27%) and C (21%). These results are in agreement with previous manuscripts [6,20–22] showing a better diagnostic accuracy of MRI with HB phase compared to DCEMRI alone, especially for lesions with Child-Pugh class A. Phongkitkarun et al. found in their high-risk population that the addition of 20-minute HB phase images increased the sensitivity from 80% (95% CI: 67–89) to 93% (95% CI: 84–98) with almost constant specificity (98%). In that series, 94/100 patients included in the study presented a Child-Pugh score A and only 1 patient showed a Child-Pugh score C [21]. Verloh et al. investigated the impact of cirrhosis grade on the diagnostic accuracy of hepato-biliary phase, using 3T MRI. They found a different relative enhancement of the liver parenchyma according to Child-Pugh grade, with an optimal HB phase at 20 minutes only for patients with Child-Pugh A score comparable to that of non-cirrhotic liver patients. Patients with Child-Pugh score B and C showed instead a delayed hepato-biliary phase, due to the reduced number of functioning hepatocytes and liver fibrosis, thus a reduced sensitivity of GD-EOB-DTPA at 20 minutes [23]. On the other hand, Van Kessel et al. suggested in patients with normal liver function a delay time of 10 minutes, instead of 20 minutes, sufficient to characterize a suspected focal liver lesion [24]. An optimal timing for lesion characterization with Gd-EOB-DTPA is not yet available. In a more recent paper, Esterson et al. evaluated in one hundred and twenty-nine patients, the effect of prolonged hepatobiliary phase delay time on hepatic enhancement in patients with parenchymal liver disease. Gd-EOB-DTPA-enhanced
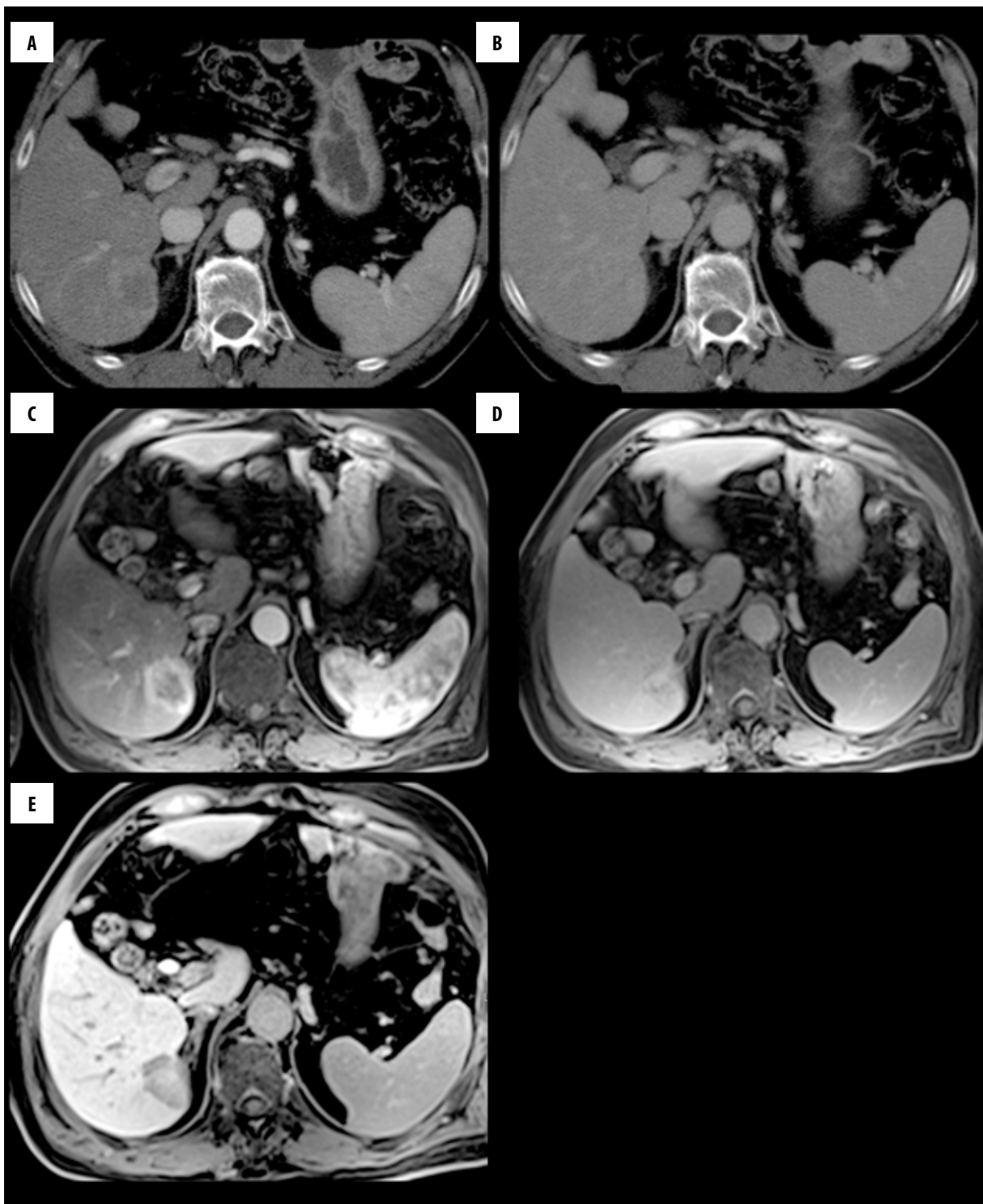
Figure 1. A 65-year-old man with hepatitis C (Child-Pugh class B) with histologically confirmed HCC. (**A**) DCECT scan obtained during the hepatic arterial phase demonstrates a 3.2-cm moderate hyper-attenuating lesion, with a central zone of necrosis in the right lobe of the liver. (**B**) Corresponding CT scan obtained during the delayed phase. (**C, D**) DCEMR images obtained during (**C**) hepatic arterial and (**D**) delayed phase. The enhancement pattern of the lesion is similar to that seen on DCECT. (**E**) Corresponding MR image obtained during the liver-specific HB phase, showing a markedly hypointense lesion compared to the highly-enhanced background liver, a finding consistent with malignancy.
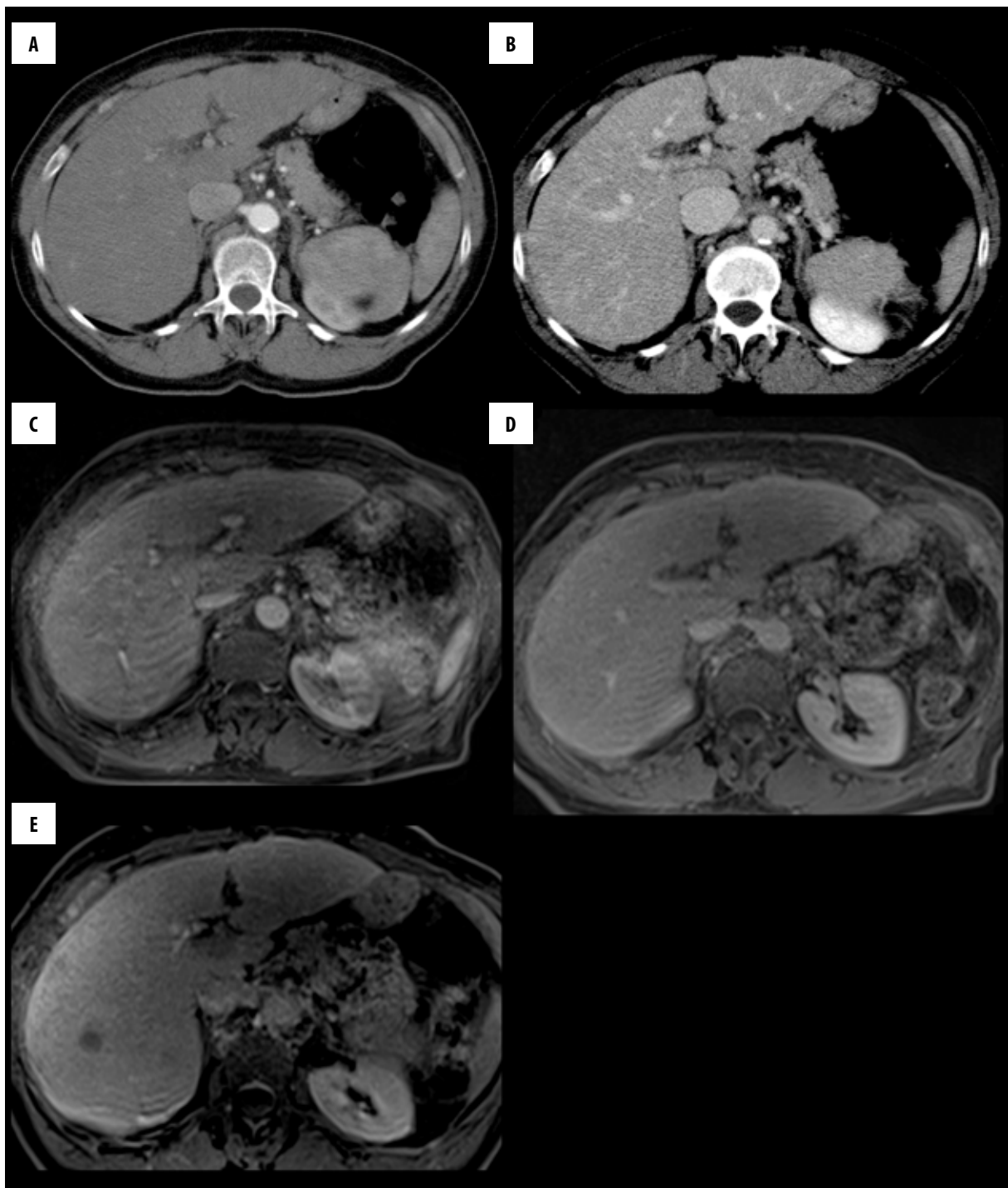
Figure 2. A 58-year-old man with hepatitis C (Child-Pugh class A) with histologically confirmed HCC. No lesions are visible during arterial (**A**) and delayed (**B**) phase of DCECT. DCEMRI confirms the absence of focal liver lesions (**C, D**). Conversely, the MR image obtained during the liver-specific HB phase, shows a markedly hypointense lesion in the VII liver segment, suggestive of malignancy (**E**).

MRI examinations with hepatobiliary phase were obtained after 20- and 30-minute delays in patients with parenchymal liver disease. The authors conclude that increasing hepatobiliary phase delay to 30 minutes improves hepatic enhancement in patients with parenchymal liver disease, particularly if using a 3T scanner. This effect is attenuated in patients with more severe end-stage liver disease [25]. Furthermore, Verloh et al. in a series of 121 patients with normal liver function and Milan end-stage liver disease (MELD) score ≤10 and 29 patients with impaired liver function and MELD score >10, demonstrated that hepatic uptake of Gd-EOB-DTPA is strongly affected by liver function and the relative enhancement during hepatobiliary phase in GD-EOB-DTPA MRI correlates with the MELD score. Therefore, assessment of relative enhancement may help improve treatment in routine clinical practice [26].
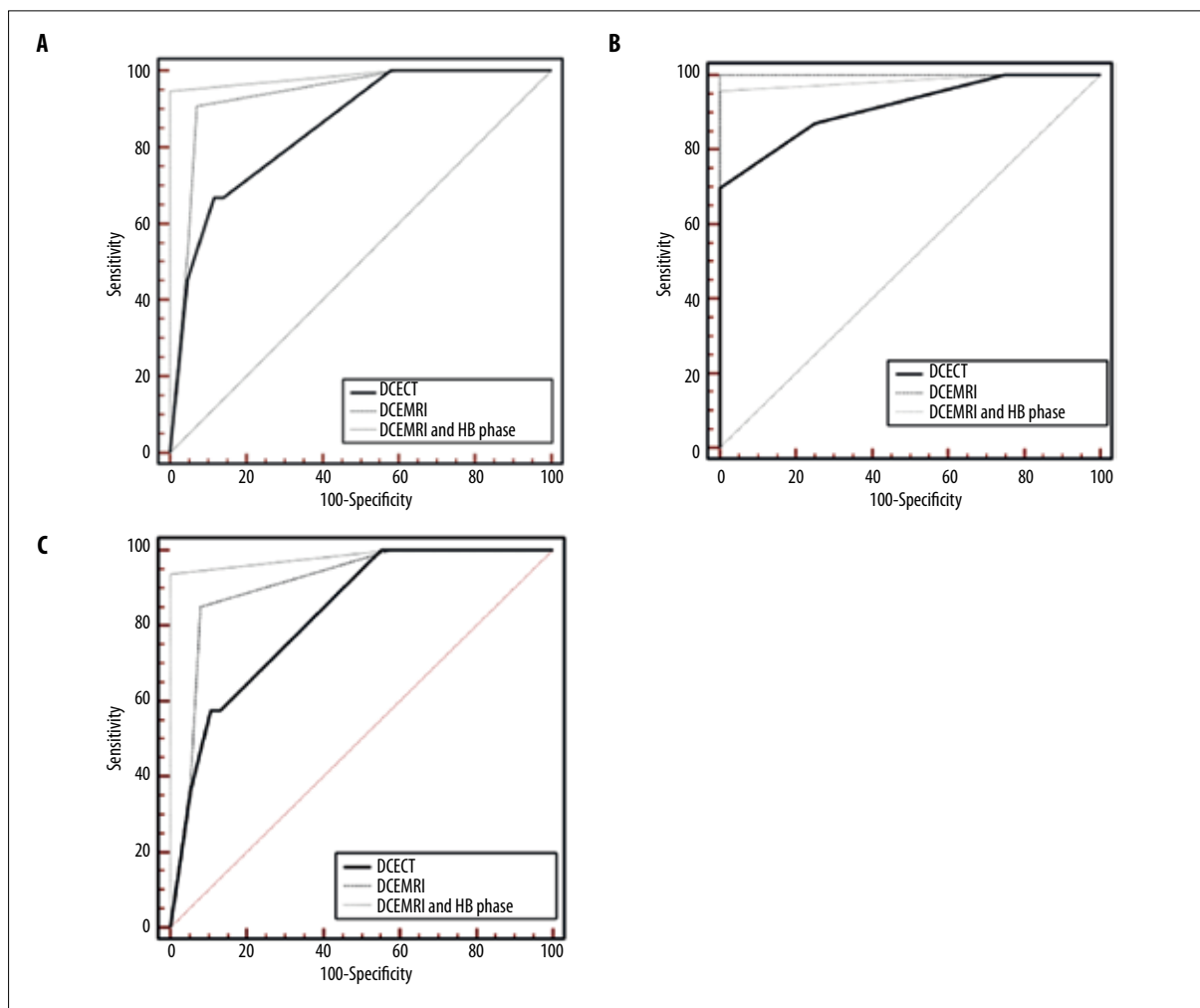
Figure 3. (**A**) ROC curves for DCECT, DCEMRI and HB phase-enhanced MRI, in the total number of lesions (n. 125). AUC value is 0.984 for DCEMRI+HB phase *vs.* 0.934 for DCEMRI (p<0.68) and 0.852 for DCECT (p<0.001). (**B**) ROC curves for DCECT, DCEMRI and HB phase-enhanced MRI, for lesions >20 mm (n. 40). No significant differences are observed among the three imaging modalities with AUC values of 0.984 for DCEMRI+HB phase, 0.999 for DCEMRI and 0.913 for DCECT. (**C**) ROC curves for DCECT, DCEMRI and HB phase-enhanced MRI, for lesions <20 mm (n. 85). AUC value is 0.982 for DCEMRI+HB phase *vs.* 0.910 for DCEMRI (p<0.01) and 0.828 for DCECT (p<0.001).

The limitation of the study was a small number of patients recruited; however, further studies in a larger patients' population are warranted to confirm the results of our manuscript.

The comparable diagnostic accuracy of GD-EOB-DTPA with MDCT and dynamic contrast-enhanced MRI in patients with advanced liver disease and Child-Pugh B or C, suggests a possible limited use of GD-EOB-DTPA only in cases of patients with less severe liver function impairment, allowing to reduce the high cost associated with the use of this "liver-specific" hepato-biliary agent.

Conclusions

The results of this study demonstrate an overall 4.5% incremental diagnostic accuracy of Gd-EOB-DTPA, compared to

the conventional technique with DCEMRI in patients with liver cirrhosis, at high risk for incidence of HCC and a superior diagnostic accuracy of MRI over CT, that is motivated by a greater contrast resolution of MRI.

The diagnostic accuracy of Gd-EOB-DTPA-enhanced MRI, significantly improves for lesions <20 mm and patients with less severe liver function impairment.

In patients with lesions >20 mm and Child-Pugh class B or C, no significant differences are observed among Gd-EOB-DTPA-enhanced MRI, DCEMRI and DCECT, due to the reduced hepatocyte function of this patient population. These findings of a lower diagnostic accuracy of GD-EOB-DTPA in patients with advanced liver disease, could be used to improve MR imaging protocols, especially given the high cost associated with the use of GD-EOB-DTPA.

References:

1. Clark HP, Carson WF, Kavanagh PV et al: Staging and current treatment of hepatocellular carcinoma. Radiographics, 2005; 25: S3–23

2. Parkin DM, Bray F, Ferlay J, Pisani P: Global cancer statistics, 2002. Cancer J Clin, 2005; 55: 74–108

3. Bruix J, Sherman M: Practice Guidelines Committee, American Association for the study of liver diseases. Management of hepatocellular carcinoma. Hepatology, 2005; 42: 1208–36

4. Colli A, Fraquelli M, Casazza G et al: Accuracy of ultrasonography, spiral CT, magnetic resonance, and alpha-fetoprotein in diagnosing hepatocellular carcinoma: A systematic review. Am J Gastroenterol, 2006; 101: 513–23

5. Cruite I, Schroeder M, Merkle EM, Sirlin CB: Gadoxetate disodium-enhanced MRI of the liver: Part 2, protocol optimization and lesion appearance in the cirrhotic liver. Am J Roentgenol, 2010; 195: 29–41

6. Park G, Kim YK, Kim CS et al: Diagnostic efficacy of gadoxetic acid-enhanced MRI in the detection of hepatocellular carcinoma: Comparison with gadopentate dimeglumine. Br J Radiol, 2010; 83: 1010–16

7. Ye F, Liu J, Ouyang H: Gadolinium ethoxybenzyl diethylenetriamine pentaacetic acid (Gd-EOB-DTPA) enhanced magnetic resonance imaging and multidetector-row computed tomography for the diagnosis of hepatocellular carcinoma: A systematic review and meta-analysis. Medicine (Baltimore), 2015; 94: e1157

8. Lee JM, Zech CJ, Bolondi L et al: Consensus report of the 4th International Forum for Gadolinium-Ethoxybenzyl-Diethylenetriamine Pentaacetic Acid Magnetic Resonance Imaging. Korean J Radiol, 2011; 12: 403–15

9. Haradome H, Grazioli L, Tinti R et al: Additional value of gadoxetic acid-DTPA-enhanced hepatobiliary phase MR imaging in the diagnosis of early stage hepatocellular carcinoma: Comparison with dynamic triple-phase multidetector CT imaging. J Magn Reson Imaging, 2011; 34: 69–78

10. Frericks BB, Loddenkemper C, Huppertz A et al: Qualitative and quantitative evaluation of hepatocellular carcinoma and cirrhotic liver enhancement using Gd-EOB-DTPA. Am J Roentgenol, 2009; 193: 1053–60

11. Akai H, Kiryu S, Matsuda I et al: Detection of hepatocellular carcinoma by Gd-EOB-DTPA-enhanced liver MRI: Comparison with triple phase 64 detector row helical CT. Eur J Radiol, 2011; 80: 310–15

12. Motosugi U, Bannas P, Sano K, Reeder SB: Hepatobiliary MR contrast agents in hypovascular hepatocellular carcinoma. J Magn Reson Imaging, 2015; 41: 251–65

13. Chen N, Motosugi N, Morisaka H et al: Added value of a gadoxetic acid-enhanced hepatocyte-phase image to the LI-RADS system for diagnosing hepatocellular carcinoma. Magn Reson Med Sci, 2016; 15: 49–59

14. Di Martino M, Marin D, Guerrisi A et al: Intraindividual comparison of gadoxetate disodium-enhanced MR imaging and 64-section multidetector CT in the detection of hepatocellular carcinoma in patients with cirrhosis. Radiology, 2010; 256: 806–16

15. Kitao A, Zen Y, Matsui O et al: Hepatocellular carcinoma: Signal intensity at gadoxetic acid-enhanced MR Imaging-correlation with molecular transporters and histopathologic features. Radiology, 2010; 256: 817–26

16. Tsuboyama T, Onishi H, Kim T et al. Hepatocellular carcinoma: Hepatocyte-selective enhancement at gadoxetic acid-enhanced MR imaging-correlation with expression of sinusoidal and canalicular transporters and bile accumulation. Radiology, 2010; 255: 824–33

17. Kitao A, Matsui O, Yoneda N et al: The uptake transporter OATP8 expression decreases during multistep hepatocarcinogenesis: Correlation with gadoxetic acid enhanced MR imaging. Eur Radiol, 2011; 21: 2056–66

18. Golfieri R, Renzulli M, Lucidi V et al: Contribution of the hepatobiliary phase of Gd-EOB-DTPA-enhanced MRI to dynamic MRI in the detection of hypovascular small (≤2 cm) HCC in cirrhosis. Eur Radiol, 2011; 21: 1233–42

19. Cha DI, Lee MW, Kim YK et al: Assessing patients with hepatocellular carcinoma meeting the Milan criteria: Is liver 3 tesla MR with gadoxetic acid necessary in addition to liver CT? J Magn Reson Imaging, 2014; 39: 842–52

20. Ahn SS, Kim MJ, Lim JS et al: Added value of gadoxetic acid-enhanced hepatobiliary phase MR imaging in the diagnosis of hepatocellular carcinoma. Radiology, 2010; 255: 459–66

21. Phongkitkarun S, Limsamutpetch K, Tannaphai P, Jatchavala J: Added value of hepatobiliary phase gadoxetic acid-enhanced MRI for diagnosing hepatocellular carcinoma in high-risk patients. World J Gastroenterol, 2013; 19: 8357–65

22. Lee YJ, Lee JM, Lee JS et al: Hepatocellular carcinoma: diagnostic performance of multidetector CT and MR imaging: A systematic review and meta-analysis. Radiology, 2015; 275: 97–109

23. Verloh N, Haimerl M, Rennert J et al: Impact of liver cirrhosis on liver enhancement at Gd-EOB-DTPA enhanced MRI at 3 Tesla. Eur J Radiol, 2013; 82: 1710–15

24. Van Kessel CS, Veldhuis WB, van den Bosch MA, van Leeuwen MS: MR liver imaging with Gd-EOB-DTPA: A delay time of 10 minutes is sufficient for lesion characterization. Eur Radiol, 2012; 22: 2153–60

25. Esterson YB, Flusberg M, Oh S et al: Improved parenchymal liver enhancement with extended delay on Gd-EOB-DTPA-enhanced MRI in patients with parenchymal liver disease: Associated clinical and imaging factors. Clin Radiol, 2015; 70: 723–29

26. Verloh N, Haemerl M, Zeman F et al: Assessing liver function by liver enhancement during the hepatobiliary phase with Gd-EOB-DTPA-enhanced MRI at 3 Tesla. Eur Radiol, 2014; 24: 1013–19